RESEARCH ARTICLE

The World's Most Popular Actinide Chelator Structurally Characterized with an Actinide: Americium Diethylenetriaminepentaacetic Acid

Brian M. Rotermund,[a,b] Nicholas B. Beck,[a] Hannah Wineinger,[a] Joseph M. Sperling, [a] Jacob P. Brannon,[a] Rosalie Greer,[c] and Thomas E. Albrecht*[a]

[a] Department of Chemistry and Nuclear Science and Engineering Center
Colorado School of Mines
Golden, Colorado 80401, USA.
*E-mail: tschoenzart@mines.edu

[b] Aqueous Separations and Radiation Chemistry Department
Idaho National Laboratory
Idaho Falls, Idaho 83415, USA.

[c] [Dept]
Savannah River National Laboratory
Jackson, South Carolina 29813, USA.

Supporting information for this article is given via a link at the end of the document

Diethylenetriaminepentaacetic acid (DTPA) is a popular chelator used prolifically in the nuclear and medical industries. However, structural data on these complexes in the solid-state have long remained elusive for the actinides. Herein, a detailed structural analysis of the presented crystal structures of $(CH_6N_3)_4$[Nd(μ-DTPA)]$_2$•nH$_2$O and $(CH_6N_3)_4$[Am(μ-DTPA)]$_2$•nH$_2$O (where $CH_6N_3^+$ is guanidinium) provides an opportunity to characterize the subtle differences in the Lewis acidity between a lanthanide/actinide pair of similar ionic sizes. Contractions in nitrogen–metal bond lengths between neodymium(III) and americium(III) were observed while the metal–oxygen bonds remain relatively consistent, highlighting the marginal favorability for actinide complexation over the lanthanides with moderately soft N-donors. Spectroscopic analysis of these complexes displayed significant splitting in many transitions and relatively strong electronic interactions with traditionally low-intensity transitions in the americium complex, as is demonstrated in the $^7F_5$ group. Pressure-induced spectroscopic analysis showed surprisingly little effect on the americium complex, with 5*f*→5*f* transitions either not shifting or marginally shifting from 2–3 nm at 11.93 ± 0.06 GPa— atypical of a soft, N-donor americium complex under pressure. Large solvent voids within the crystal structure could be responsible for the lack of pressure response in these crystals. **[177 words]**

Introduction [764 words]

Within the nuclear industry, separation of the minor actinides (americium and curium) is often a difficult hurdle to overcome, as these predominantly trivalent actinides share very similar chemical properties to the intermixed lanthanide fission products. Despite this challenge, separation of these problematic actinides offers the benefits of: (i) significantly reducing the radiothermal and radiotoxic burden of used nuclear fuel (UNF) for disposal; (ii) isolating americium for industrial applications, such as radioisotope thermoelectric generators for use in space exploration; and (iii) enabling the disposal of the minor actinides *via* transmutation.[1–3]

Furthermore, the need for rapid medical care is essential to keep radiological workers safe from highly hazardous materials in the event of worker contamination. Internal exposure to radiotoxic materials such as the actinides poses significant risk to the radiological workers handling such materials. Internal contamination by actinide materials is known to displace metal ions and concentrate in particular areas of the body (e.g., displacing calcium in the bones and protein and cellular interactions within the liver) and cause substantial biological damage through the generation of ionizing radiation.[4–6] As such, immediate and effective treatment is essential for decorporation of these elements from the body. This is often achieved by chelation therapy, in which a strong chelating ligand is injected into the body to displace and complex the actinide, after which it is excreted.

Championed as a class of excellent metal chelators, aminopolycarboxylates (APCs) have long been and continue to be heavily utilized in rare earth, nuclear, and medical industries. Among them, diethylenetriaminepentaacetic acid (DTPA) stands out for its high affinity for the trivalent lanthanides and actinides, making DTPA desirable for the separation of these elements. This ligand has been explored for use within multiple reprocessing technologies/flow sheets, such as TALSPEAK (Trivalent Actinide Lanthanide Separation with Phosphorus-reagent Extraction from Aqueous Komplexes), GANEX (Group ActiNide EXtraction), ALSEP (Actinide-Lanthanide SEParation), and EXAm (EXtraction of Americium) among other tail-end PUREX (Plutonium Uranium Reduction EXtraction) processes.[7–13] DTPA looks to exploit the softer Lewis acid character of the actinides relative to the lanthanides through bonding of the ethyleneamine backbone to the metal ion. The softer N-donor atoms of DTPA show slight preference to the actinides over the harder lanthanides, allowing

for separation by liquid-liquid extraction. Similarly, in chelation therapy, this strong affinity for the trivalent actinides over that of common biological metal ions found in the body facilitates efficient actinide decorporation.

With the prolific use of DTPA across multiple industries being intimately acquainted with actinides, it is understandable that many studies have been focused on their interactions with The utility of DTPA *f*-element complexes has encouraged a wide variety of investigations into their coordination environment, including thermodynamic calculations and molecular modeling, spectroscopy, and Extended X-ray Absorption Fine Spectrum (EXAFS).[14–18]. While XAS studies can provide broad details about coordination environment such as hydration, speciation, and coordination numbers, the bond length data extracted from EXAS is limited and subject to a larger margin of error. In contrast, single-crystal X-ray crystallography (SC-XRD) is unmatched in its ability to provide highly detailed modeling of structural information on coordination modes, bond lengths, and bond angles of a complex. Crystallographic studies are pivotal for developing an encompassing view on the bonding behavior between a metal and a ligand, yet there has never been a crystallographically characterized actinide-DTPA compound.

The lack of actinide DTPA structural characterization is surprising given its prolific involvement with americium among other trivalent actinides and its detailed structural study with trivalent lanthanides. A crystallographic study on americium(III) DTPA would provide detailed atomic-level insight on the coordinating behavior of actinides with DTPA and pave the way for future computational studies on actinide-APC interactions.

With these points in mind, we present the crystallographic characterization of $(CH_6N_3)_4[Nd(\mu\text{-DTPA})]_2\bullet n H_2O$ and $(CH_6N_3)_4[Am(\mu\text{-DTPA})]_2\bullet n H_2O$; highlighting the subtle crystallographic and structural differences between americium and its ionic radius lanthanide congener, neodymium. Spectroscopic analysis of these DTPA structures was carried out with solution phase UV-vis-NIR and compared to solid-state absorption spectra under ambient and low temperature (93.15 K) conditions. The solid-state absorption spectroscopy was studied as a function of pressure up to 11.93 ± 0.06 GPa using a Diamond Anvil Cell (DAC). These measurements provide insight into the effects of hard-soft character interactions between that of the harder neodymium ion and the softer americium ion based on their spectroscopic shifting.

Results and Discussion [1872 words]

$(CH_6N_3)_4[Nd(\mu\text{-DTPA})]_2\bullet n H_2O$ crystallizes in the monoclinic space group $P2_1/n$ and consists of a single DTPA ligand coordinating through five carboxylate oxygens and three nitrogen atoms in the diethylenetriamine backbone, giving an 8-coordinate DTPA complex in the asymmetric unit. This complex holds an overall 2− charge, balanced by two guanidinium cations. However, a large opening remains in the inner coordination sphere of the neodymium metal ion when observed in the asymmetric unit. A symmetry-generated carboxylate oxygen is coordinated in this coordination sphere opening, revealing a dimeric complex, shown in **Figure 1**, where each metal center is 9-coordinate bridging through O1 and O1a. Such coordination environments are not expected in solution, however, as this opening in the coordination sphere is typically occupied by water.[13]

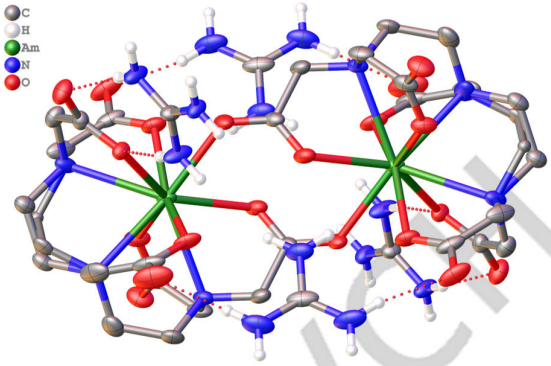

Figure 1. Dimer moiety of Americium DTPA. Hydrogens on the DTPA ligand excluded for clarity. Theral ellipsoid probablity at 50%.

Disorder is observed in the diethylenetriamine backbone, shown in **Figure 2**, where one of these ethylene groups is positionally disordered in a gauche fashion with torsion angles of 56.8(7)° for N21–C91–C101–N3 and −73.7(12)° for N21–C92–C102–N3. Based off the free crystallographic occupancy of each orientation, these conformations hold an occupancy of 0.65 (orientation 1) and 0.35 (orientation 2), respectively. This disorder propagates through the ethyleneamine, splitting the central tertiary amine and continuing to the acetic acid groups of O5–O6–C7–C8 (carboxylate 3), where orientation 2 extends out closer to the symmetry generated complex. The carboxylate of O9–O10–C13–C14 (carboxylate 4) shows similar splitting with orientation 2 extending closer to the dimer complex. The geometry around the metal center varies between muffin and a spherical capped square antiprism geometry for orientation 1 and orientation 2, respectively.

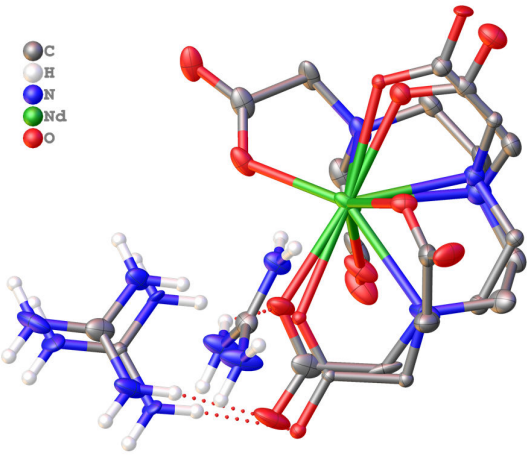

Figure 2. Asymmetric unit of the neodymium DTPA complex displaying positional disorder. Hydrogens on the DTPA ligand excluded for clarity. Theral ellipsoid probablity at 50%.

Between carboxylate 3 and 4, a guanidinium cation also showed splitting, shifting in relation to the position of carboxylate 3 and 4 with hydrogen bonding observed between the disordered

guanidinium hydrogens and the disordered carboxylates. The second guanidinium in the asymmetric unit exhibits hydrogen bonding with O101 and O102, but when observing the crystal packing habits, this guanidinium displays additional inter-dimeric H-bonding between O1, O7, O8, O91, and O92a. Looking along the b axis reveals a H-bonding network from this guanidinium, connecting the dimer complexes *via* a 2-dimensional network. A void between dimer complexes exists containing water molecules which could not be crystallographically resolved. Applying a solvent mask to this void found 116 electrons within this 422 Å^3 void, equating to approximately 11.6 water molecules in the void.

Average metal–oxygen bond lengths within the NdDTPA asymmetric unit measured at 2.460(16) Å. Metal coordinated atoms which held positional disorder within the structure (O6 and O10) saw larger than average deviation in their bond lengths and larger errors. The bond length between the bridging O1a atom and the neodymium metal center is slightly longer than the average observed with a bond length of 2.496(3) Å. Metal–nitrogen bond lengths are notably longer than the metal-oxygen bonds observed, which is expected for metal–nitrogen bonds with an average of 2.674(13) Å. The Nd1–N22 bond length of 2.585(10) Å is uncharacteristically short compared to the other metal–nitrogen bonds, likely due to the high degree of disorder from the split nitrogen positions. This bond is notably shorter than its split Nd1–N21 counterpart that falls within expected neodymium–nitrogen bond lengths at 2.699(7) Å.

$(CH_6N_3)_4[Am(\mu\text{-DTPA})]_2\bullet n H_2O$ is isostructural to the neodymium complex and crystallizes in the monoclinic space group $P2_1/n$ and displays the same coordination behavior as neodymium, showing a 9-coordinate americium complex, including the O1a coordination from the symmetry generated complex to form the dimer. The local geometry around the americium metal ion is a muffin geometry. The complex again holds a 2– charge with two guanidinium cations positioned in the outer sphere of the complex for charge balance.

There are indications of similar disorder within the americium complex as was seen in the neodymium structure. Two carbon atoms in the ethyleneamine backbone, C9 and C10, are again disordered in a gauche fashion with torsion angles of 59.7(5)° for N2–C91–C101–N3 and −82.4(13)° N2– C92–C102–N3. Crystallographic occupancies differ from the neodymium structure, showing a 0.75 favorability towards orientation 1 and 0.25 for 2. This disorder does not propagate through the rest of the structure as it does in the neodymium carboxylate groups. There are indications that this positional disorder still exists, although to a lesser extent, by the presence of elongated ellipsoids. However, this disorder was not resolvable.

The guanidinium cations are positioned in a very similar manner to the neodymium structure. One guanidinium is positioned between O9 and O5a, exhibiting hydrogen bonding the guanidinium and the carboxylate groups on either side. The other guanidinium cation displays similar behavior as the neodymium structure, where hydrogen bonding with O10 is observed. When viewing the extended structure, inter-dimeric hydrogen bonding is again observed between O1, O7, O8, and O9. Looking along the b axis again shows the 2-D network, demonstrated in **Figure 3**, connecting through hydrogen bonding of these guanidinium cations. A void again exists between the dimer complexes with a volume of 444 Å^3, containing 244 electrons. A solvent mask was applied equating to 24.4 water molecules in the void. The large increase in electron density within this void, despite the the voids across both structures holding a relatively similar in size, shows

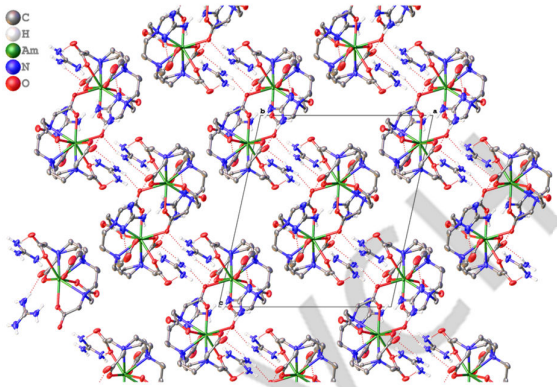

Figure 3. Lattice view of americium DTPA looking along the b-axis. Hydrogens on the DTPA ligand excluded for clarity. Theral ellipsoid

that the organization of these structures is dominated by the complex and cation packing; indicating that solvent molecules have negligible impact on the crystal organization of these systems.

Metal–oxygen bond lengths of the americium DTPA complex are similar to those seen in the neodymium structure. Average metal–oxygen bond lengths measure at 2.452(7) Å with the Am1–O1a bond length also being similar to that in the neodymium structure at 2.499(3) Å. Metal–nitrogen bond lengths are also similar to those observed in the neodymium structure with an average bond length of 2.672(6) Å.

Solution phase absorption spectrum of $(CH_6N_3)_4[Nd(\mu\text{-DTPA})]_2\bullet n H_2O$, **Figure S6**, displays in high resolution the splitting of $4f\rightarrow4f$ transitions, allowing many peaks to be individually identified be identified. Most transitions display a bathochromic shift when coordinated to DTPA compared to the historically reported transitions in the neodymium halides.[19] The solid-state absorption spectrum of $(CH_6N_3)_4[Nd(\mu\text{-DTPA})]_2\bullet n H_2O$ (**Figure S7**) displays many of the same features observed in the solution phase absorption spectrum with some regions, such as the 800 nm region displaying increase splitting of overlapping $4f\rightarrow4f$ transitions. However, due to the low signal to noise ratio in the solid-state spectrum, the lower intensity transitions are not identifiable.

A comparison of solution phase absorption spectra of the americium(III) chloride and the americium(III) DTPA solutions (**Figure S8**) displays very similar electronic behavior with a few key differences. The $[AmDTPA]^{2-}$ absorption complex exhibits a slight bathochromic shift of about 4 nm up to the $^5L_6$ (504 nm) transition. The $^7F_6$ (~810 nm) transition splits to two distinct peaks while the $^7F_4$ (1050 nm) single peak is split into several low intensity transitions. The peaks in the $^7F_5$ (860 – 915 nm area) transitions make no appearance in the chloride absorption spectrum but do appear with low intensity in the $[AmDTPA]^{2-}$ absorption spectrum.

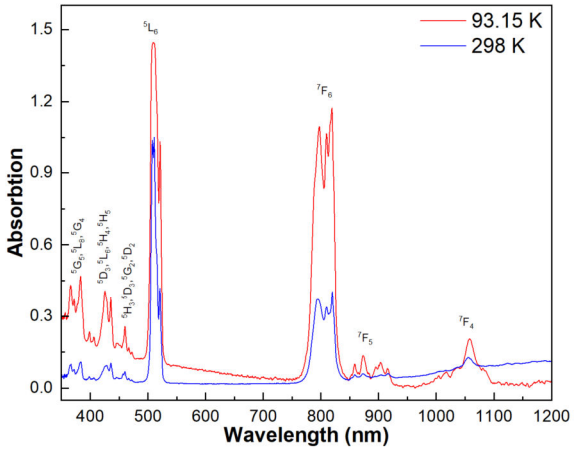

Figure 4. Solid-state absoroption spectra of $(CH_6N_3)_4[Am(\mu\text{-}DTPA)]_2{\bullet}nH_2O$ at low temperatuer (Red) and under ambient conditions (blue).

Solid-state absorption spectra of $(CH_6N_3)_4[Am(\mu\text{-}DTPA)]_2{\bullet}nH_2O$ (**Figure 4**) display much more detail in the high energy region (350 nm to 480 nm), due the absence of the water solvent cutoff absorbing the low intensity 5*f*→5*f* transitions. The $^5L_6$ transition has now split into two to three distinct peaks. Interestingly, splitting appears to decrease at low temperature with two peaks coalescing into a single peak, contrary to what is typically observed, as splitting of transitions often increases in solid-state absorption spectra at low temperatures.[20] The $^7F_6$ region shows additional splitting from the solution state spectrum with three distinct peaks and, at cold temperatures, shoulders are apparent in the 819 nm peak. The low intensity transitions in the $^7F_5$ region show sharp intensities, displaying at least five distinct peaks. While the $^7F_4$ transition shows increased sharpness, additional features in this region are difficult to distinguish from the lower signal to noise ratio resulting from the temperature-controlled stage use for measurements of these samples at cold temperature.

High pressure spectroscopy of $(CH_6N_3)_4[Am(\mu\text{-}DTPA)]_2{\bullet}nH_2O$ (**Figure 5**) was measured to observe the effective differences in the hard-soft nature of the Lewis acidity of lanthanides versus actinides based on the influence of pressure on each respective complex's absorption spectra. [INSERT MISSING Nd PRESSURE DATA].

Within the $[AmDTPA]^{2-}$ complex, all transitions that experience shifting do so in a bathochromic fashion, while some transitions exhibit no effect at all from applied pressure. Of notable transitions, the $^5L_6$ region displays four peaks with the shoulder between the 511 nm and the 521 nm peak becoming more prominent under light (0.21 ± 0.04 – 4.13 ± 0.04 GPa) pressure and gradually merging into the 508 nm and 511 nm doublet, which experience bathochromic shifting 2.0 nm and 3.1 nm, respectively, before coalescing into a single peak with a centroid at approximately 512 nm. The 521 nm peak exhibits some bathochromic shifting of 2.3 nm, however, by 4.13 ± 0.04 GPa the transition does not shift any further and remains at this position, decreasing in intensity and broadening. Interestingly, the transitions in the $^7F_6$ region display no shifting whatsoever. The transitions within this region remain constant until 11.93 ± 0.06 GPa where the intensities of the *f*→*f* transitions decrease and broaden until they coalesce into a single broad transition. Similar to the $^7F_6$ region, the $^7F_5$ transitions also displays no change when pressure is applied, vanishing into the baseline after 8.48 ± 0.04 GPa. Finally, the $^7F_4$ region again displays bathochromic shifting of 5.7 nm before broadening to where the transition vanishes within the baseline.

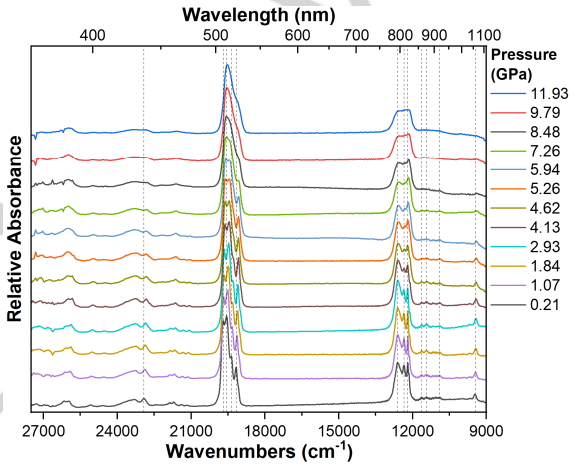

Figure 5. High pressure solid-state absorption spectrum $(CH_6N_3)_4[Am(\mu\text{-}DTPA)]_2{\bullet}nH_2O$ with pressure applied via a diamon anvil cell (DAC).

Interestingly, the americium complex exhibits 5*f*→5*f* transition shifting comparable to that of the neodymium complex. Given the presence of softer N-donor atoms within the DTPA ligands, a greater degree of spectroscopic shifting was expected in the americium complex, as the softer 5*f* elements should see greater interaction with soft donor atoms to affect their respective spectroscopy as pressure is applied. However, instead we observe little to no shifting across all significant transitions within the spectra and significantly less spectroscopic shifting of other reported americium compounds under pressure, even in exclusively O-donor systems.[21,22] One such cause of these observations could stem from the effects of the solvent voids under pressure. Initial application of pressure could compress the voids, causing a slight redistribution of atoms around the complex as indicated by the initial shifting of some transitions up to 4.13 ± 0.04 GPa. However, the high number of water molecules within these voids could reach a limit of compression as pressure is applied to these crystal lattices, where the void reaches an incompressible state. This limits the pressure exerted on the crystal lattice and distributes pressure away from the metal complex, explaining why some transitions stop shifting after a few

GPa. Some more "open" regions of the complex, such as the space between the dimers, could be more susceptible to the applied pressure and could explain why some transitions continue to be affected up to the 11.93 ± 0.06 GPa maxima.

Conclusion

Here, we have reported the synthesis of a DTPA complex with americium and its neodymium congener. These structures crystallized to form a dimerized complex taking the formula $(CH_6N_3)_4[M(\mu\text{-DTPA})]_2 \bullet n H_2O$. These 9-coordinate metal ion complexes take either a muffin or spherical capped square antiprism geometry for the neodymium complex and muffin for the americium complex. Each complex contains a void contain water molecules with the americium crystal structure hold a much higher electron density over the neodymium structure. The fact that these complexes see isomorphic coordination despite very different void conditions shows that the organization of the crystal lattice hold no dependence on the surrounding solvent. Both complexes displayed significant 5*f*→5*f* splitting and a relatively increased intensity with transitions which are typically low intensity. The $(CH_6N_3)_4[Am(\mu\text{-DTPA})]_2 \bullet n H_2O$ structure exhibits a limited response to pressure up to 11.93 ± 0.06 GPa, likely as a result of the incompressible solvent voids.

Supporting Information

The authors have cited additional references within the Supporting Information.[23–25]

Acknowledgements

This work was supported by the U.S. Department of Energy (DOE), Office of Sciences, Office of Basic Energy Sciences, Solar Photochemistry Program Award, DE-SC0024191. The isotopes used in this research were supplied by the U.S. DOE Isotope Program, managed by the Office of Science for Isotope R&D and Production.

Keywords: DTPA • Pentaacetic acid • Americium • Actinides • Chelation

References

(1) Taiwo, T. A.; Kim, T. K.; Stillman, J. A.; Hill, R. N.; Salvatores, M.; Finck, P. J. Assessment of a Heterogeneous PWR Assembly for Plutonium and Minor Actinide Recycle. *Nucl. Technol.* **2006**, *155* (1), 34–55. https://doi.org/10.13182/NT06-A3744.

(2) Ambrosi, R.; Williams, H.; Samara-Ratna, P.; Tomkins, K.; Pulker, S.; Slade, R.; Bannister, N.; Stephenson, K.; Simpson, K.; Robbins, M.; Dimitriadou, I.; Reece, M.; Ning, H.; Chen, K.; Perkinson, M.-C.; Sykes, J.; Rice, T.; Tinsley, T.; Sarsfield, M.; Vernon, D.; Crawford, T.; Stuttard, M.; Koenig, J.; Jaegle, M. Americium-241 Radioisotope Thermoelectric Generator Development for Space Applications; Brazil, 2013; Vol. 45.

(3) Wigeland, R. A.; Bauer, T. H.; Fanning, T. H.; Morris, E. E. Separations and Transmutation Criteria to Improve Utilization of a Geologic Repository. *Nucl. Technol.* **2006**, *154* (1), 95–106. https://doi.org/10.13182/NT06-3.

(4) Keith, S.; Ingerman, L.; McCartney, R. A.; Chappell, L. L.; Wohlers, D. W.; Sage, G. W.; Diamond, G. L.; Neal, M. *Toxicological Profile for Americium*; Toxicology Profile PMID 37816099; Agency for Toxic Substances and Disease Registry (US): Atlanta, GA, USA, 2004; pp 15–102. https://www.ncbi.nlm.nih.gov/books/NBK595689/.

(5) Belanger, R. Plutonium. In *Encyclopedia of Toxicology*; Elsevier: Amsterdam, NL, 2005; Vol. 1, pp 450–452.

(6) Lindenbaum, A.; Rosenthal, M. W. Deposition Patterns and Toxciticty of Plutonium and Americium in the Liver. *Health Phys.* **1972**, *22* (6), 597–605. https://doi.org/10.1097/00004032-197206000-00009.

(7) Weaver, B.; Kappelmann, F. A. Preferential Extraction of Lanthanides over Trivalent Actinides by Monoacidic Organophosphates from Carboxylic Acids and from Mixtures of Carboxylic and Aminopolyacetic Acids. *J. Inorg. Nucl. Chem.* **1968**, *30* (1), 263–272. https://doi.org/10.1016/0022-1902(68)80089-2.

(8) Weaver, B.; Kappelmann, F. A. *TALSPEAK: A New Method of Separating Americium and Curium from the Lantahnides by Extraction from an Aqueous Solution of an Aminopolyacetic Acid Complex with a Monoacidic Organophosphate or Phosphonate*; Technical Information Document ORNL-3559; Oak Ridge National Laboratory: Oak Ridge, Tennessee, United States of America, 1964; pp 1–61. https://www.osti.gov/servlets/purl/4028257-IPYQDU/.

(9) Miguirditchian, M.; Vanel, V.; Marie, C.; Pacary, V.; Charbonnel, M.-C.; Berthon, L.; Hérès, X.; Montuir, M.; Sorel, C.; Bollesteros, M.-J.; Costenoble, S.; Rostaing, C.; Masson, M.; Poinssot, C. Americium Recovery from Highly Active PUREX Raffinate by Solvent Extraction: The EXAm Process. A Review of 10 Years of R&D. *Solvent Extr. Ion Exch.* **2020**, *38* (4), 365–387. https://doi.org/10.1080/07366299.2020.1753922.

(10) Lumetta, G. J.; Gelis, A. V.; Carter, J. C.; Niver, C. M.; Smoot, M. R. The Actinide-Lanthanide Separation Concept. *Solvent Extr. Ion Exch.* **2014**, *32* (4), 333–347. https://doi.org/10.1080/07366299.2014.895638.

(11) Kosyakov, V. N.; Yerin, E. A. Separation of Transplutonium and Rare-Earth Elements by Extraction with HDEHP from DTPA Solutions. *J. Radioanal. Chem.* **1978**, *43*, 37–51. https://doi.org/10.1007/BF02519439.

(12) Choppin, G. R. Structure and Thermodynamics of Lanthanide and Actinide Complexes in Solution. *Pure Appl. Chem.* **2009**, *27* (1–2), 23–41. https://doi.org/10.1351/pac197127010023.

(13) Zalupski, P. R.; Grimes, T. S.; Pilgrim, C. D.; Heathman, C. R.; Jansone-Popova, S.; Johnson, K. R.; Bryantsev, V. S.; Chapleski Jr., R. C. *Aminocarboxylates in Trivalent F-Element Separations*; Handbook on the Physics and Chemistry of the Rare Earths; Elsevier: Amsterdam, NL, 2021; Vol. 60.

(14) Rizkalla, E. N.; Sullivan, J. C.; Choppin, G. R. Calorimetric Studies of Americium(III) Complexation by Amino Carboxylates. *Inorg. Chem.* **1989**, *28* (5), 811–982. https://doi.org/10.1021/ic00304a022.

(15) Tian, G.; Martin, L. R.; Zhang, Z.; Rao, L. Thermodynamic, Spectroscopic, and Computational Studies of Lanthanide Complexation with Diethylenetriaminepentaacetic Acid: Temperature Effect and Coordination Modes. *Inorg. Chem.* **2011**, *50* (7), 3087–3096. https://doi.org/10.1021/ic200025s.

(16) Kimura, T.; Choppin, G. R. Luminescence Study on Determination of the Hydration Number of Cm(III). *J. Alloys Compd.* **1994**, *213–214*, 313–317. https://doi.org/10.1016/0925-8388(94)90921-0.

(17) Kimura, T.; Kato, Y. Luminescence Study on Hydration States of Lanthanide(III)–Polyaminopolycarboxylate Complexes in Aqueous Solution. *J. Alloys Compd.* **1998**, *275–277*, 806–810. https://doi.org/10.1016/S0925-8388(98)00446-0.

(18) Deblonde, G. J.; Kelley, M. P.; Su, J.; Batista, E. R.; Yang, P.; Booth, C. H.; Abergel, R. J. Spectroscopic and Computational Characterization of Diethylenetriaminepentaacetic Acid/Transplutonium Chelates: Evidencing Heterogeneity in the Heavy Actinide (III) Series. *Angew. Chem. Int. Ed.* **2018**, *57* (17), 4521–4526.

(19) Carnall, W. T.; Fields, P. R.; Rajnak, K. Electronic Energy Levels in the Trivalent Lanthanide Aquo Ions. I. Pr3+, Nd3+, Pm3+, Sm3+, Dy3+, Ho3+, Er3+, and Tm3+. *J. Chem. Phsyics 49* (10), 4424–4442. https://doi.org/10.1063/1.1669893.

(20) Pappalardo, R. G.; Carnall, W. T.; Fields, P. R. Low-Temperature Optical Absorption of Americium Halides. *J. Chem. Phsyics* **1969**, *51* (3), 1182–1200. https://doi.org/10.1063/1.1672121.

(21) Rotermund, B. M.; Beck, N. B.; Sperling, J. M.; Horne, G. P.; Huffman, Z. K.; Grödler, D.; Albrecht, T. E. Comprehensive Synthesis and Structural Trends in Tetramethyl Diglycolamide (TMDGA) Nitrate Complexes with Lanthanides and Americium. *Cryst. Growth Des.* **2024**, *24* (21), 8855–8865. https://doi.org/10.1021/acs.cgd.4c00869.

(22) Sperling, J. M.; Warzecha, E.; Klamm, B. E.; Gaiser, A. N.; Windorff, C. J.; Whitefoot, M. A.; Albrecht-Schönzart, T. E. Pronounced Pressure Dependence of Electronic Transitions for Americium Compared to Isomorphous Neodymium and Samarium Mellitates. *Inorg. Chem.* **2020**, *60* (1), 476–483. https://doi.org/10.1021/acs.inorgchem.0c03293.

(23) Sheldrick, G. M. Crystal Structure Refinement with SHELXL. *Acta Crystallogr. Sect. C* **2015**, *71* (1), 3–8. https://doi.org/10.1107/S2053229614024218.

(24) Sheldrick, G. M. SHELXT - Integrated Space-Group and Crystal-Structure Determination. *Acta Crystallogr. Sect. A* **2015**, *71* (1), 3–8. https://doi.org/10.1107/S2053273314026370.

(25) Dolomanov, O. V.; Bourhis, L. J.; Gildea, R. J.; Howard, J. A. K.; Puschmann, H. OLEX2: A Complete Structure Solution, Refinement and Analysis Program. *J. Appl. Crystallogr.* **2009**, *42*, 339–341. https://doi.org/10.1107/S0021889808042726.

Entry for the Table of Contents

((Insert graphic for Table of Contents here (300 DPI resolution: up to 650x532 pixels for single-column format; up to 1358x295 pixels for double-column format). Please ensure your graphic is in **one** of the two following formats.))

((max. width: 5.5 cm; max. height: 4.5 cm))
650x532 pixels
Please delete this box prior to submission.

or

((max. width: 11.0 cm; max. height: 2.5 cm))
1358x295 pixels
Please delete this box prior to submission.

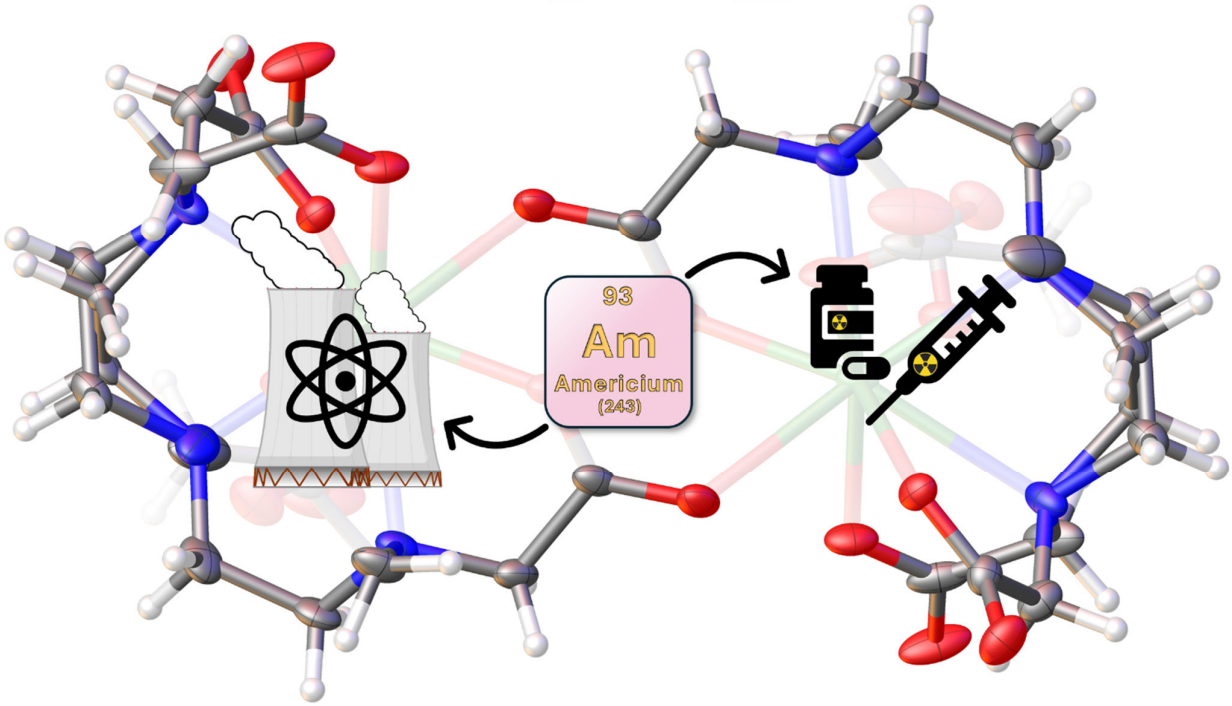

Insert text for Table of Contents here. ((Maximum 450 characters including spaces; please provide a Table of Contents text that gives readers a short preview of the main theme of the research and results included in the paper to attract their attention into reading the paper in full. Define acronyms, including those in the picture! The Table of Contents text should be different from the abstract.))

Institute and/or researcher Twitter usernames: ((optional))